ERCOFTAC Bulletin No. 72, 2007, pp.61-66

Implicit Large-Eddy Simulations of Wall-Bounded Turbulent Flows

Dimitris Drikakis*, Marco Hahn, Zeshan Malick, Evgeniy Shapiro
Fluid Mechanics and Computational Science Group,
Department of Aerospace Sciences
Cranfield University, Cranfield MK43 0AL, United Kingdom.

Abstract

The paper presents application of Implicit Large Eddy Simulation (ILES) to wall-bounded turbulent flows. A characteristics-based scheme in conjunction with total variation diminishing (TVD) Runge-Kutta time stepping and slope-limiting variants, for the compressible flow case, have been employed. Results are presented for an incompressible lid-driven cavity flow, using an incompressible solver, and low-Mach number flows over a hill and around a delta wing, using a compressible solver. Good agreement with experimental data and numerical results using classical LES has been obtained. Future ILES developments are also discussed.

1 Introduction

Given the capabilities of today's supercomputers it is not possible to compute turbulent flows directly by resolving fully each turbulent eddy motion in space and time, thus part of the unsteady/turbulent motion must be approximated to make these calculations feasible. The grand challenge is to develop simulation models that although may not be explicitly incorporating all dynamic eddy scales of the flow, will still give accurate and reliable results for at least the large energy-containing scales of motion. The computational challenge is thus to solve these model equations as accurately as possible. The current drive is towards Large Eddy Simulation (LES) in which the large energy containing structures are resolved, whereas the smaller, more isotropic, structures are filtered out and, therefore, their effects need to be modelled, e.g. [1]. This gives LES a much higher generality than industrial-standard Reynolds Averaged Navier-Stokes (RANS) approaches, which solve equations averaged over time, spatially homogeneous directions, or across an ensemble of equivalent flows, and for which the entire turbulent spectrum is effectively modelled.

Different approaches are available for deriving the LES equations and the associated subgrid scale (SGS) models required to handle the effects of the unresolved flow physics. In general, we need to distinguish between classical and implicit LES. In classical LES the Navier-Stokes equations are filtered by convolving all dependent variables with a predefined filter in order to extract the large scale components, see e.g. [2] for a recent survey. Classical approaches have ranged from the inherently-limited subgrid viscosity formulations, to more sophisticated and accurate dynamic and mixed models - of limited popularity given their implementation and computational complexity. In the context of classical LES and in the absence of a universal theory of turbulence, the construction of SGS models is unavoidably pragmatic, and based primarily on the rational use of empirical information. Difficulties pertinent to classical LES have been discussed in recent surveys ([1], [3]) and include commutation and aliasing errors, limitations with regard to compressible flows and masking of the SGS terms by the truncation error.

The ILES approach (see [4] for a recent survey) employs the original (unfiltered) flow equations instead of the filtered ones and the effects of the SGS physics on the resolved scales are incorporated in the functional reconstruction of the convective fluxes using high-resolution finite-volume methods (as defined by Harten [5]). The ILES methods invoke non-oscillatory constraints via non-linear limiters to implicitly act as a filtering (and non-linear adaptive regularization) mechanism for the small scales. Modified equation analysis indicates that the leading truncation-error terms introduced by such methods provide implicit SGS models of mixed anisotropic type [6]. Attempts to formalise the development of ILES numerical schemes is hindered by the inherent complexity of theoretical analysis of non-linear schemes, however, recent developments show some good agreements between truncation errors due to the numerical scheme and the required form of the subgrid terms [7]. Major properties of the implicit SGS model are related to: (i) the choice of high- and low-order schemes - where the former is well-behaved in smooth flow regions, and the latter is well-behaved near sharp gradients; (ii) the choice of flux/slope-limiter which determines how these schemes should be blended locally, depending on prescribed characterisation of the flow smoothness; (iii) the balance of the dissipation and dispersion contributions to the numerical solution, which strongly depend on the design details of each numerical method. Using ILES, excellent results have been gained in simulation of flows as varied as Rayleigh-Taylor and Richtmyer-Meshkov instability [8, 9, 10], free jets [11, 12], channel flow [12], open cavity flow [3, 13], geophysical flows [14, 15], delta wings [16] and decaying turbulence [6, 17, 18, 19, 20].

Wall-bounded flows are present in many industrial applications. Classical LES becomes prohibitively expensive in near-wall high-Reynolds number flows thus hybrid approaches such as hybrid LES/RANS and detached eddy simulation (DES) have emerged as alternatives. With regard to the transfer of information across the RANS and LES boundaries, both hybrid RANS/LES and DES lack theoretical justification since time-averaging in RANS and spatial filtering in LES are unrelated operations. Additionally, the constraints posed by classical LES also apply to the hybrid approaches with respect to the LES component of the simulation. Coupling of ILES with unsteady RANS would not encompass the same uncertainties since ILES is based on the unfiltered equations. Alternatively, an even more challenging option would be to numerically integrate the equations using ILES throughout the do-

*Corresponding author, d.drikakis@cranfield.ac.uk. The authors' names appear in alphabetical order.

main. In respect of this, a (small) number of studies concerning the accuracy of ILES in wall-bounded flows have been conducted [6, 13, 21, 22, 23].

We have developed several ILES variants ranging from third-order TVD methods [24] to ninth-order WENO schemes [25] in conjunction with several different non-linear slope-limiting schemes. In this paper, we present results from a second/third-order ILES variant based on the characteristics-based (CBS) scheme, which is applicable to both incompressible and compressible flows [24, 26, 27]. Results from high-order implementations will be presented in a future paper. In the incompressible case, the CBS implementation is based on the artificial compressibility approach [26, 28, 29]. For the lid-driven cavity flow, the time integration was performed using a fourth-order Runge-Kutta scheme, while for the low-Mach number flows over a hill and around a delta wing an extended stability third-order Runge-Kutta scheme was employed (see [26] for a recent survey on these methods).

2 Lid-driven Cavity Flow

Prasad and Koseff [30] performed a series of experiments providing extensive Laser Doppler Anemometry data for laminar ($Re = 3,200$), transitional ($Re = 5,000 - 7,500$) and fully turbulent ($Re = 10,000$) regimes. In the lid-driven cavity flow, the viscous interactions not only dominate the small-scale behaviour in the near-wall region but also provide the driving force by transferring momentum from the moving lid.

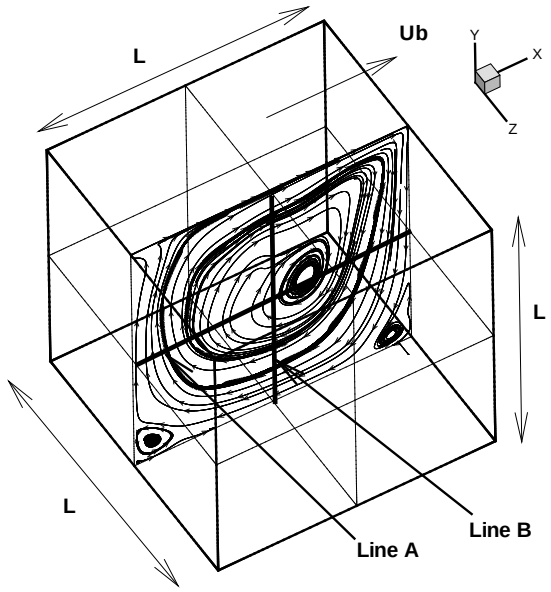

Figure 1: Schematic of the lid-driven cavity case.

Computations have been conducted for the fully turbulent case at $Re = 10,000$ based on the lid velocity and cavity height. A 64^3 grid was employed with hyperbolic clustering near the wall, e.g. [31]. Following the experimental measurements of Prasad and Koseff [30], the comparison between computations (labelled as 'CBS') and experiment is obtained along lines A and B as per Figure 1. The CBS scheme has been implemented in conjunction with 1st, 2nd and 3rd order variable interpolation[1]. In all figures the results have become dimensionless using the lid velocity, U_b, and characteristic time of the lid motion, L/U_b.

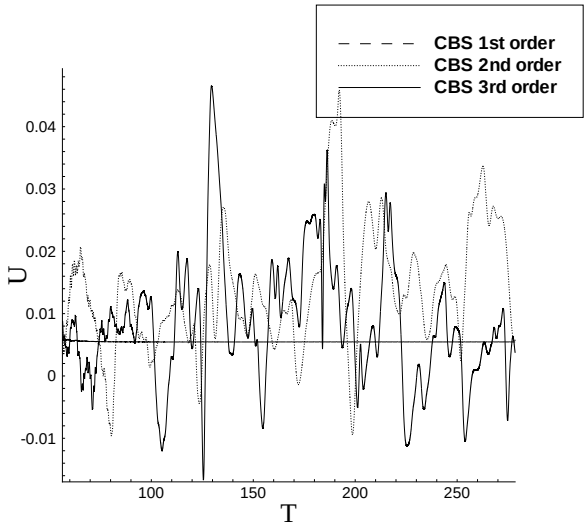

Figure 2: Time trace of instantaneous velocity at 5mm above the lower wall along line B. The first-order variant gives very small fluctuations, due to excessive dissipation, which are not visible on the figure scale.

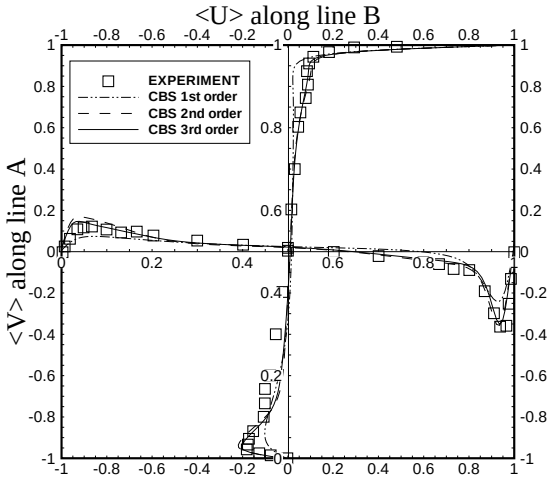

Figure 3: Mean velocity profiles.

The ILES computation was initialised using a laminar flow solution obtained for $Re = 3,200$. The turbulent flow computation was carried out until the flow establishes a turbulent behaviour similar to the experiment (Figure 2). Two hundred dimensionless time units were found sufficient to establish converged turbulent statistics. Time-averaged velocities were computed within this time window. Figure 3 shows averaged velocity components in the x and y directions; $\langle V \rangle$ denotes time-averaged y-velocity along line A and $\langle U \rangle$ averaged x-velocity along line B, respectively. The results obtained using second and third-order CBS variants are in very good agreement with the experimental profiles. The first-order variant is less accurate, as expected, due to excessive dissipation.

The results for the turbulent fluctuation, $\langle V_{rms} \rangle$, are shown in Figure 4. Greater discrepancies are observed

[1]Strictly speaking only the 1st order interpolation variant yields a monotonic scheme

in the middle of the cavity due the coarseness of the grid in this region (the grid is clustered near the walls), as well as in the peak value of turbulent fluctuation near the moving lid.

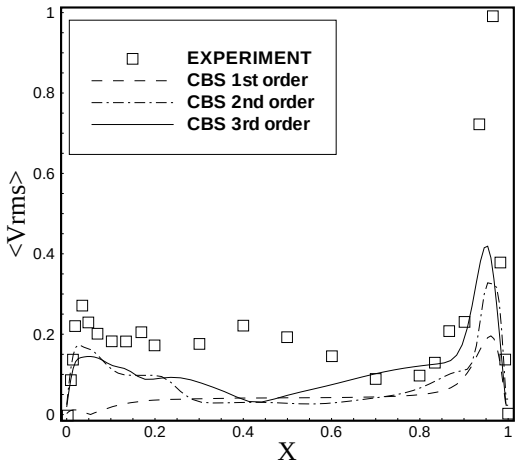

Figure 4: $V_{rms} = 10\sqrt{\langle V'^2 \rangle}$ along line A

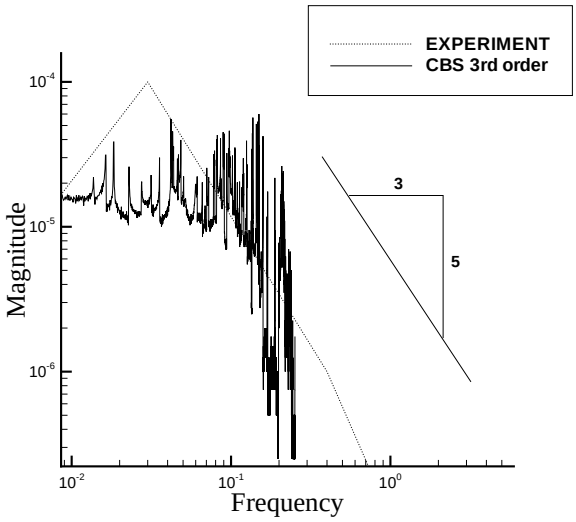

Figure 5: Velocity power spectrum

The velocity power spectra has been computed using a discrete Fourier transform of the velocity fluctuation at position 5mm above the lower wall along line B, which coincides with the point of velocity peak due to the appearance of the Taylor-Gortler-like (TGL) vortices. As can be seen from the results in Figure 5, the spectra slope is compared favourably with the experimental data of [30].

3 Hill flow

Another well-established example of a simple wall-bounded flow is the "hill" flow that consists of a channel with hill-type curvature on the lower wall (Figure 3). The flow features separation on the downwind slope. The computational domain was $9h \times 4.5h \times 2h - 3h$ (h is the height of the constriction) in the streamwise, cross-stream and wall-normal directions, respectively. The simulations were conducted using a compressible code (CNS3D) based on the CBS method and a second/third-order slope-limiting scheme [24]. The Reynolds number based on the bulk velocity at the hill crest was equal to $10,595$ and the Mach number was 0.2. No-slip boundary conditions are applied on the top and bottom walls of the channel, while periodicity was assumed in the streamwise and cross-stream directions.

Since pressure-driven channel flow violates the periodicity constraint, a modified version of the external forcing term given by Lenormand et al. [32] was employed in order to ensure a constant mass flow rate. The computational grid comprised $112 \times 91 \times 64$ cells with grid spacing of $\Delta x/h = 0.080, \Delta y/h = 0.049, \Delta z/h = 0.032$ at the hill crest, which corresponds to a highly under-resolved simulation. The grid clustering normal to the bottom wall can also be described in non-dimensional wall units, ranging from $z^+ \approx 5$ in the trough to $z^+ \approx 10$ at the crest.

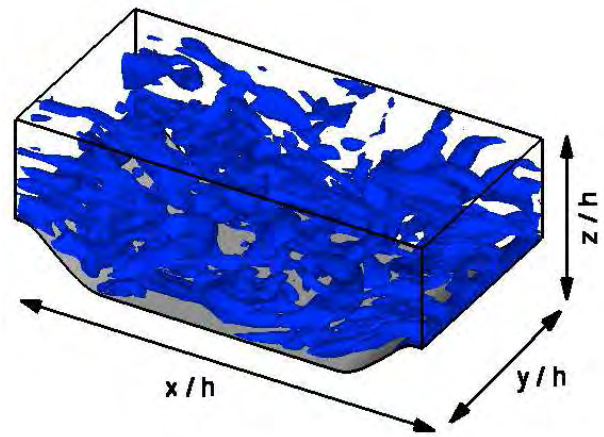

Figure 6: Computational domain and instantaneous vortical structures in the channel.

Comparison of ILES and classical LES (using the WALE SGS model) [33] is shown in Figure 7. The comparison concerns under-resolved simulations on identical grids using the present ILES approach (labelled as "CNS3D"), classical LES approach without a wall model (labelled as "STREAMLES"), and classical LES in conjunction with a two-layer logarithmic wall model (labelled as "STREAMLES LL2"). STREAMLES NS corresponds to the reference solution of a wall-resolved LES with no-slip boundary condition [33].

The averaged streamwise velocity profiles obtained by ILES and classical LES without a wall model are nearly identical with minor differences near the top and bottom of the channel. This confirms the validity of the pressure forcing term employed in the ILES simulation. The slight discrepancies on the wall can be attributed to the use of different post-processing techniques; in the ILES case the output is processed with respect to the grid vertices, whereas in the classical LES with reference to the cell-centred values. The two-layer logarithmic wall model leads to a better agreement of the velocity profile with respect to the reference solution thus seemingly improves the result. However, the analysis of stresses reveals that the second-order statistics are only weakly affected. Classical LES with and without a wall model significantly over-predict the stress magnitude, whereas ILES predicts the peak turbulent stress much closer to the well-resolved LES. The location of

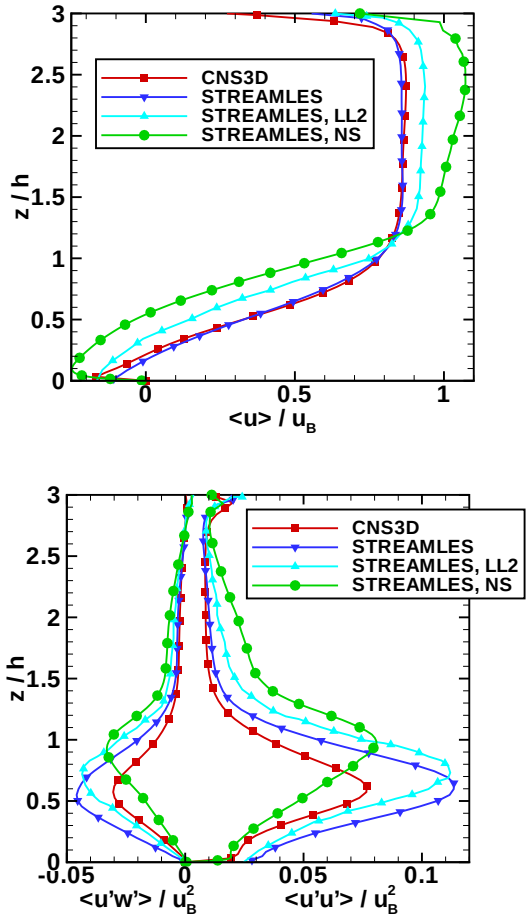

Figure 7: Averaged streamwise velocities (top) and turbulent stresses (bottom) at $x/h = 2$ as predicted by ILES (CNS3D) and classical LES (STREAMLES).

the shear layer is highly dependent on the point of separation from the gently curved hill surface. Both ILES and classical LES (without a wall model) delay separation in the under-resolved case, while the use of the LL2 wall model marginally improves the results.

The assumption of a logarithmic boundary layer profile does not hold in this case where the recirculation zone on the lee side of the hill has a major influence on the flow. As shown by Temmerman et al. [33], the results obtained by the classical LES can be improved by changing the shape of the wall function. However, ILES might not need to resort to a wall model in order to successfully predict the turbulent statistics if the separation point is well resolved (by using a finer grid) or the curvature is less gentle.

4 Delta wing

ILES simulations of the flow around a flat-plate delta wing with a leading edge sweep angle of $\Lambda = 50°$, have also been conducted. The flow features shear-layers and complex vortical structures pertinent to aeronautical applications. Symmetry was assumed along the root chord and the resulting H-H-type grid consists of 660,000 grid points spanning a three-dimensional domain of size $8c \times 3c \times 6c$ (c is the root chord length of the delta wing) in x-direction (chordwise), y-direction (spanwise) and z-direction (normal), respectively. The grid has been clustered in the vicinity of the wing, where $\Delta x/c$ is $\mathcal{O}(10^{-2})$, $\Delta y/c$ is $\mathcal{O}(10^{-2})$ and $\Delta z/c$ is $\mathcal{O}(10^{-4})$ near the surface. This should be considered as a highly under-resolved simulation with respect to the grid. The same method (and computer code) as in the hill-flow case was also used here.

The angle of incidence was $\alpha = 10°$, the Mach number was 0.2 and the Reynolds number based on the free-stream velocity and the root chord length was 26,000 as per the experiment of Taylor et al. [34, 35] and direct numerical simulations (DNS) by Gordnier & Visbal [16], performed on a computational grid of 4.5M points.

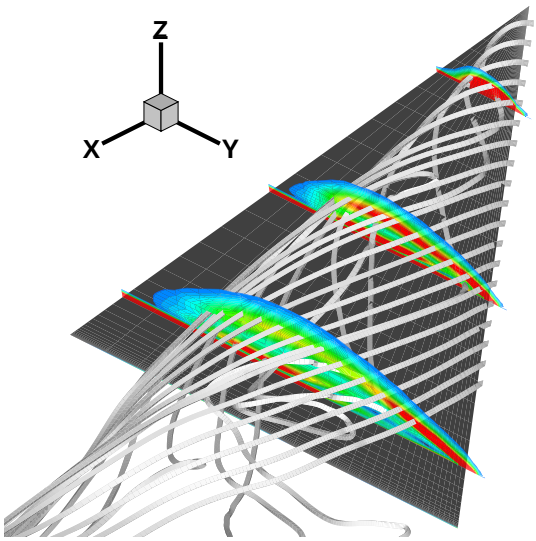

Figure 8: Instantaneous streamlines and iso-vorticity contours.

Figure 8 shows instantaneous streamlines and iso-vorticity contours obtained by the ILES simulation. The sharp leading-edge (LE) provides a well-defined separation line. Consequently, the shear-layer emanating from the LE rolls up and a stable leading edge vortex (LEV) system develops. Breakdown of the LEV and the associated reversed flow in the vortex core can be observed just downstream of the trailing edge.

Averaged contours of axial (streamwise) velocity and cross-flow velocity vectors in a plane normal to the wing surface at approximately one third of the root chord, are shown in Figure 9. The LEV is often found by applying a minimum vorticity criterion, but here the minimum axial velocity (dark region) is used to locate its centre. According to the above, the position of the vortex core as predicted by DNS [16], marked by a white cross in the figure, matches with the results of the under-resolved ILES simulation.

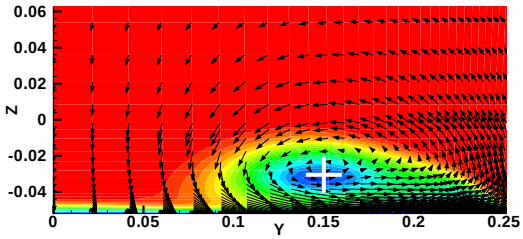

Figure 9: Averaged position of the vortex core, (based on the minimum of axial velocity), at $x/c = 0.3$ as predicted by ILES (CNS3D) and DNS [16] (white cross).

Figure 10 illustrates the averaged axial velocity in a plane through the vortex core. The experimental results [35] are compared with the contours obtained by ILES (CNS3D). The extent of the primary LEV as predicted by ILES is found in satisfactory agreement with the experiment. However, the secondary vortex which appears towards the trailing edge could not be predicted. This can be attributed to the coarseness of the mesh in this region. The DNS simulations of Gordnier & Visbal [16] have shown that a distinctive dual-vortex system exists for lower angles of attack, whereas at an incidence of $\alpha = 15^o$ a single primary vortex has been observed. For the present case of $\alpha = 10°$, only an extremely weak secondary vortex occurs.

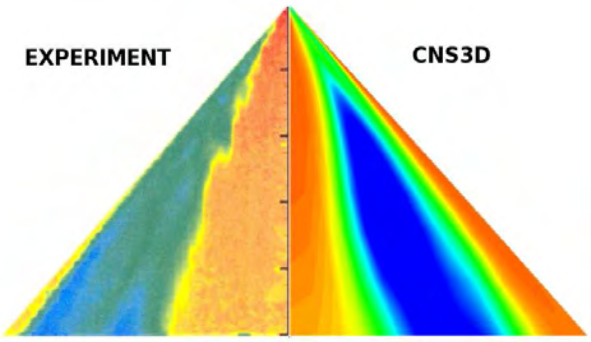

Figure 10: Comparison of the averaged axial velocity in a plane through the vortex core as predicted by ILES (CNS3D) and experiment [35].

The above results show that ILES can capture the correct physics and large-scale dynamics of a non-slender, flat-plate delta wing flow, in an under-resolved grid environment. However, secondary separation and finer structures require finer grids and/or higher than third-order of accuracy.

5 Conclusions

Results from ILES studies for a broad range of fully turbulent wall-bounded flows such as lid-driven cavity flow, separated hill flow and flow around a delta wing, were presented. The results were obtained using incompressible and compressible ILES at low Mach numbers.

For the lid-driven cavity flow good agreement was obtained against the experiment with regard to the averaged velocities and turbulent velocity spectrum, however the magnitude of the turbulent stresses is underestimated. In the separated hill flow case, ILES results for the turbulent shear stresses are in closer agreement with the wall-resolved LES simulation than the corresponding results obtained by classical LES, with and without a wall model. In the delta-wing case, ILES results are in good agreement with DNS with respect to the location of the vortex-core.

Overall, application of ILES to wall-bounded turbulent flows, shows that such flows can be computed without resorting to explicit wall modelling. Current and future work concerns the implementation of higher-order ILES variants (up to ninth-order of accuracy) and theoretical studies of the properties of ILES methods in the near wall-region of transitional and turbulent flows.

Acknowledgements: The financial support from EPSRC, BAE SYSTEMS, MOD, and UKAEA are greatly acknowledged. The authors would like to thank L. Temmerman for the provision of classical LES results and further information regarding the hill flow case.

Bibliography

[1] S. B. Pope. *Turbulent Flows*. Cambridge University Press, 2000.

[2] P. Sagaut. *Large-eddy simulation for incompressible flows - An introduction*. Springer-Verlag, 2005.

[3] D.Drikakis. Advances in turbulent flow computations using high-resolution methods. *Prog. Aerosp. Sci.*, 39:405–424, 2003.

[4] F. F. Grinstein, L.G. Margolin, and W. J. Rider, editors. *Implicit Large Eddy Simulation*. CUP, 2006.

[5] A. Harten, B. Engquist, S. Osher, and S.R. Chakravarthy. Uniformly high order accurate essentially non-oscillatory schemes, III. *J. Comput. Phys.*, 71(2):231–303, 1987.

[6] C. Fureby and F.F. Grinstein. Large Eddy Simulation of High-Reynolds-Number Free and Wall-Bounded Flows. *J. Comput. Phys.*, 181:68–97, 2002.

[7] L.G. Margolin, W.J. Rider, and F.F. Grinstein. Modeling Turbulent Flow with Implicit LES. *J. Turbul.*, 7(15):1–27, 2006.

[8] D.L. Youngs. Application of MILES to Rayleigh-Taylor and Richtmyer-Meshkov Mixing. *AIAA-2003-4102*, 2003.

[9] D.L. Youngs. Three-dimensional numerical simulation of turbulent mixing by Rayleigh-Taylor instability. *Phys. Fluids A*, 3(5):1312–1320, 1991.

[10] B. Thornber and D. Drikakis. ILES of Shock Waves and Turbulent Mixing using High Resolution Riemann Solvers and TVD Methods. In *ECCOMAS 2006,Minisymposia on Large Eddy Simulation: Theory and Applications*, 2006.

[11] J.P. Boris, F.F. Grinstein, E.S. Oran, and R.L. Kolbe. New insights into large eddy simulation. *Fluid Dyn. Res.*, 10:199–228, 1992.

[12] F.F. Grinstein and C. Fureby. Recent progress on miles for high reynolds number flows. *J. Fluid Eng.-T. ASME*, 848:848–861, 2002.

[13] M. Hahn and D. Drikakis. Large eddy simulation of compressible turbulence using high-resolution method. *Int. J. Numer. Meth. Fl.*, 49:971–977, 2005.

[14] L.G. Margolin, P.K. Smolarkiewicz, and Z. Sorbjan. Large-eddy simulations of convective boundary layers using nonoscillatory differencing. *Physica D*, 133:390–397, 1999.

[15] P.K. Smolarkiewicz and L.G. Margolin. MPDATA: a finite difference solver for geophysical flows. *J. Comput. Phys.*, 140(2):459–480, 1998.

[16] R.E. Gordnier and Visbal M.R. Compact Difference Scheme Applied to Simulation of Low-Sweep Delta Wing Flow. *AIAA J.*, 43:1744–1752, 2005.

[17] D. Drikakis, C. Fureby, F. Grinstein, M. Hahn, and D. Youngs. MILES of transition to turbulence in the taylor-green vortex system. In *ERCOFTAC Workshop on Direct and Large Eddy Simulation-6*, page 133, 2006.

[18] C. Fureby, F. Tabor, H.G. Weller, and A.D. Gosman. A comparative study of subgrid scale models in homogeneous isotropic turbulence. *Phys. Fluids*, 9(5):1416–1429, 1997.

[19] D.H. Porter, P.R. Woodward, and A. Pouquet. Inertial range structures in decaying compressible turbulent flows. *Phys. Fluids*, 10(1):237–245, 1998.

[20] L.G. Margolin, P.K. Smolarkiewicz, and A.A. Wyszogrodzki. Implicit turbulence modelling for high reynolds number flows. *J. Fluids Eng.*, 124:862–867, 2002.

[21] S. Sherer and M. Visbal. Implicit Large Eddy Simulations Using a High-Order Overset Grid Solver. *AIAA-2004-2530*, 2004.

[22] H. Yan, D. Knight, and A. A. Zheltovodov. Large-Eddy Simulation of Supersonic Flat-Plate Boundary Layers Using the Monotonically Integrated Large-Eddy Simulation (MILES) Technique. *J. Fluids Eng.*, 124:868–875, 2002.

[23] S. Hickel and N.A. Adams. ALDM - A modelling environment for ILES. In *Proceedings of ECCOMAS CFD*, 2006.

[24] J. Zóltak and D. Drikakis. Hybrid upwind methods for the simulation of unsteady shock-wave diffraction over a cylinder. *Computer Methods in Applied Mechanics and Engineering*, 162:165–185, 1998.

[25] D.S. Balsara and C.-W. Shu. Monotonicity preserving weighted essentially non-oscillatory schemes with increasingly high order of accuracy. *J. Comput. Phys.*, 160:405–452, 2000.

[26] D. Drikakis and W. Rider. *High-Resolution Methods for Incompressible and Low-Speed Flows.* Springer, 2004.

[27] A. Eberle. Characteristic flux averaging approach to the solution of the Euler equations. Technical report, VKI Lecture Series, 1987.

[28] D. Drikakis, P. A. Govatsos, and D. E. Papantonis. A Characteristic-Based Method for Incompressible Flows. *International Journal for Numerical Methods in Fluids*, 19:667–685, 1994.

[29] E. Shapiro and D. Drikakis. Non-conservative and conservative formulations of characteristics-based schemes. *Int. J. Num. Meth. Eng.*, 66(9):1466–1482, 2006.

[30] A.K. Prasad and J.R. Koseff. Reynolds number and end-wall effects on a lid-driven cavity flow. *Phys. Fluids*, 1:208–218, 1989.

[31] P.R. Eiseman. A multi-surface method of coordinate generation. *J. Comput. Phys.*, 33:118–150, 1979.

[32] E. Lenormand, P. Sagaut, L. Ta Phuoc, and P. Comte. Subgrid-Scale models for Large-Eddy Simulations of compressible wall bounded flows. *J. AIAA*, 38(8), 2000.

[33] L. Temmerman, M.A. Leschziner, C.P. Mellen, and J. Fröhlich. Investigation of wall-function approximations and subgrid-scale models in large eddy simulation of separated flow in a channel with streamwise periodic constrictions. *Int. J. Heat Fluid Flow*, 24:157–180, 2003.

[34] G.S. Taylor, T. Schnorbus, and I. Gursul. An investigaton of vortex flows over low sweep delta wings. *AIAA-2003-4021*, 2003.

[35] G.S. Taylor and I. Gursul. Unsteady vortex flows and buffeting of a low sweep delta wing. *AIAA-2004-1066*, 2004.